ACS APPLIED MATERIALS & INTERFACES

Research Article

www.acsami.org

Structurally and Electronically Designed TiO_2N_x Nanofibers for Lithium Rechargeable Batteries

Jae-Geun Kim,[†,‡] Dongqi Shi,[‡] Ki-Jeong Kong,[†,§] Yoon-Uk Heo,[†,⊥] Jung Ho Kim,*[,‡] Mi Ru Jo,[#] Yoon Cheol Lee,[#] Yong-Mook Kang,*[,#] and Shi Xue Dou[‡]

[‡]Institute for Superconducting and Electronic Materials, University of Wollongong, Innovation Campus, North Wollongong, NSW 2500, Australia

[§]NanoBio Fusion Research Center, Korea Research Institute of Chemical Technology, Daejeon 305-343, Republic of Korea

[⊥]Research Facility Center, Graduate Institute of Ferrous Technology, Pohang University of Science and Technology, Pohang 790-784, Republic of Korea

[#]Department of Energy and Materials Engineering, Dongguk University-Seoul, Seoul 100-715, Republic of Korea

Supporting Information

ABSTRACT: The morphology and electronic structure of metal oxides, including TiO_2 on the nanoscale, definitely determine their electronic or electrochemical properties, especially those relevant to application in energy devices. For this purpose, a concept for controlling the morphology and electrical conductivity in TiO_2, based on tuning by electrospinning, is proposed. We found that the 1D TiO_2 nanofibers surprisingly gave higher cyclic retention than 0D nanopowder, and nitrogen doping in the form of TiO_2N_x also caused further improvement. This is due to higher conductivity and faster Li^+ diffusion, as confirmed by electrochemical impedance spectra. Our findings provide an effective and scalable solution for energy storage efficiency.

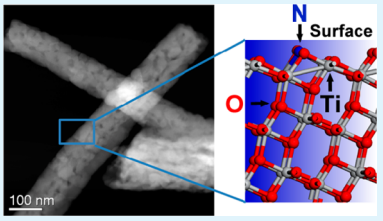

KEYWORDS: *titanates, nitrogen doping, electrospinning, lithium ion batteries, 1D nanostructure, TiO_2N_x*

INTRODUCTION

Titanium dioxide, TiO_2, is a window semiconductor material for photocatalysts, photovoltaic cells, gas sensors, and other electrochemical devices,[1,2] because of its wide band gap (3.2 eV), cost-effectiveness, and nontoxic nature. In particular, rationalizing the morphology of TiO_2 undoubtedly plays a key role in enhancing its electronic or electrochemical performance. From the viewpoint of an electrode material for the lithium rechargeable battery, TiO_2 can yield a considerable advantage in terms of its rate performance governed by electronic conductivity, as well as in electrochemical versatility because of its various polymorphs. TiO_2 has been well-known to have diverse polymorphs such as anatase, rutile, brookite, TiO_2 B, TiO_2 R, TiO_2 H, TiO_2 II, and TiO_2 III.[3−14] On the basis of a previous report,[2,14] the TiO_2 B polymorph is an ideal host for Li^+ intercalation because it has a relatively open tunnel structure compared to anatase, rutile, and brookite. Anatase also has the same sort of mesoporous structure, and in addition, its long voltage plateau obtained during Li^+ insertion/extraction is definitely ideal for use in lithium rechargeable batteries. However, repeated charge and discharge tend to quickly drive down the capacity of anatase due to its poor Li^+ conductivity and electronic conductivity. Recently, spinel lithium titanate, $Li_4Ti_5O_{12}$, has been considered as the most promising anode material for achieving the extremely high rate performance required for application in electric vehicles and short life-cycle energy storage systems.[15−18] Even so, because TiO_2 has not only higher theoretical capacity (335 mA h g^{-1}) but also apparently morphological and structural versatility, the research on TiO_2 is very likely to make a breakthrough on its application in lithium rechargeable batteries for novel energy applications such as electric vehicles and energy storage systems. As various synthetic methods have been suggested with the development of nanotechnology, it might be expected that the lithium storage performance of polymorph TiO_2 nanostructures could be superior to the current state-of-the-art performance if a favorable architecture for electron or Li^+ transport is found. To achieve these aims, the one-dimensional (1D) nanostructure has been regarded as one of the most promising types. In particular, the 1D architecture has received great attention due to not only its unique structural characteristics, but also because of its tunable intrinsic properties,[19−22] i.e., Li^+ intercalation and conductivity. For this purpose, application of the electrospinning process can be suggested as an easy and economical way to improve the lithium storage performance of TiO_2 because of the merits of 1D structure that are associated with it, such as facilitated ion transport and enhanced electronic conductivity. Electrospinning is not only a relatively simpler approach compared to other complicated synthetic methods (chemical vapor deposition (CVD), physical vapor deposition (PVD), etc.) for 1D nanomaterials, but also a versatile method for obtaining various kinds of fibrous structure. Furthermore,

Received: October 3, 2012
Accepted: January 10, 2013
Published: January 10, 2013

the 1D nanostructure obtained through electrospinning strongly tends to feature uniform diameter and diverse compositions.[23,24] So, it enables homogeneous coating or doping to enhance the electrical conductivity,[25] whatever the original inorganic nanomaterials are. In this study, therefore, we systematically report the role of 1D architecture (see Scheme S1 in the Supporting Information) and nitrogen doping on the lithium storage properties of TiO_2 in rechargeable batteries. Moreover, we answer the effect of nitrogen doping clearly: where does nitrogen, what is formed and why electrochemical performance properties are improved? Our findings provide atomic-level insight and electric structure, which could pave the way to further enhancement of performances in the lithium ion battery up to the theoritical limit.

EXPERIMENTAL SECTION

Preparation of Bare TiO_2 and TiO_2N_x Nanofibers and Structural Characterization. For the two kinds of TiO_2 nanofibers, 1.5 g of titanium isopropoxide was mixed with ethanol and 0.5 mL of acetic acid. After 1 h, this solution was added into 5 mL of ethanol, containing of 4.5 wt % polyvinylpyrrolidone (PVP), followed by magnetic stirring for 1 h. For nitrogen-doped TiO_2 nanofibers, 0.1 mL of diethylenetriamine as nitrogen source was added to the Ti precursor solution. With increasing amount of diethylenetriamine, we found a small fraction of rutile phase. The yellow transparent spinning solution was immediately loaded into a plastic syringe equipped with a 23 gauge needle. The needle was connected to a high voltage supply, and the feeding rate for the precursor was set at 0.5 mL h^{-1} (see Figure S1 in the Supporting Information). A distance of 9 cm and voltage of 15 kV (see Figure S2 in the Supporting Information) were maintained between the tip of the needle and the drum collector. After the electrospinning, the as-spun nanofibers were left in air for 24 h to obtain anatase TiO_2 nanofibers. The nanofibers were heat-treated in air at 450 °C for 1 h to remove PVP. The morphology and structure of the nanofibers were characterized by field emission-scanning electron microscopy (FE-SEM), and transmission electron microscopy (TEM). Nitrogen doping into TiO_2 was further studied by using X-ray photoelectron spectroscopy (XPS) and FTIR (Vertex 80 V, Bruker, Germany).

Electrochemical Performance. Coin-type half cells (CR2016) were assembled to evaluate the anodic performances of the two kinds of 1D TiO_2 nanofibers and the TiO_2 nanoparticles. In this experiment, 1D TiO_2 nanofibers or TiO_2 nanoparticles were used as the active electrode. Each electrode was fabricated by mixing each active material, acetylene black, and polyvinylidene fluoride (PVDF) at a weight ratio of 75:17:8 using N-methylpyrrolidone (NMP) as a solvent. After coating the slurry on Al foil, they were dried at 120 °C for 5 h under vacuum. The assembly was carried out in an Ar-filled glovebox with less than 0.1 ppm each of oxygen and moisture. Li metal foil was used as the counter and reference electrode, and 1 M $LiPF_6$ dissolved in a 1:1 (by volume) mixture of ethylene carbonate (EC) and diethyl carbonate (DEC) was employed as the electrolyte. A polypropylene (PP) film was used as separator. Charge (Li^+ insertion)-discharge (Li^+ extraction) tests were performed up to the 40 cycles in the range of 1 to 3 V (vs Li/Li^+). Electrochemical impedance spectroscopy (EIS) analysis of the coin half-cells were performed using a Iviumstate potentiostat/galvanostat (Ivium Technologies, Netherlands). The EIS frequency ranged from 100 kHz to 0.1 Hz and the EIS ac perturbation amplitude was 5 mV for room temperature measurements. Data acquisition and analysis were done respectively using the electrochemical impedance software, ZPlot and Zview (Version 3.0, Scribner Associates, Inc., USA).

First Principles Calculations. Spin-polarized density functional theory (DFT) calculations were performed using the periodic plane wave approach, as implemented in the Vienna Ab-initio Simulation Package (VASP) code[26,27] in the generalized gradient approximation (GGA) using the Perdew-Burke-Ernzerhof (PBE) exchange-correlation functional.[28] Frozen-core projector augmented wave pseudopotentials were used.[29,30] A special 3 × 3 × 1 k-point sampling was applied for the surface Brillouin zone integration. The plane wave basis set was restricted by the cutoff energy of 400 eV. The anatase (101) surface was modeled with a periodically repeated slab of four TiO_2 layers (twelve atomic layers) separated by a vacuum of 20 Å width. We considered a super cell containing 96 atoms, with surface cell parameters u = 10.972 Å, v = 7.569 Å, α = 110.18°. These optimized lattice parameters are taken from another calculation on bulk anatase phase. Total energies are converged to 1×10^{-6} eV. All structures were fully optimized, with the largest residual force smaller than 0.01 eV $Å^{-1}$. The atoms in the bottom layer were fixed to their bulk positions during geometry optimizations, in order to simulate the presence of the bulk underneath.

RESULTS AND DISCUSSION

The configuration and crystalline microstructure of the bare and nitrogen-doped TiO_2 fibers produced in this work can be directly seen in the scanning electron microscope (SEM) and high-magnification transmission electron microscope (TEM) images in Figure 1. In images a and b in Figure 1, the diameters of the two kinds of fibers were estimated to be 100−200 nm. Interestingly, there was no noticeable change through nitrogen doping. The morphology of the two types of TiO_2 fibers was further observed by bright-field TEM, as shown in images c and d in Figure 1. The fiber surface obtained was smooth and uniform. We were able to conclusively prove that the two kinds

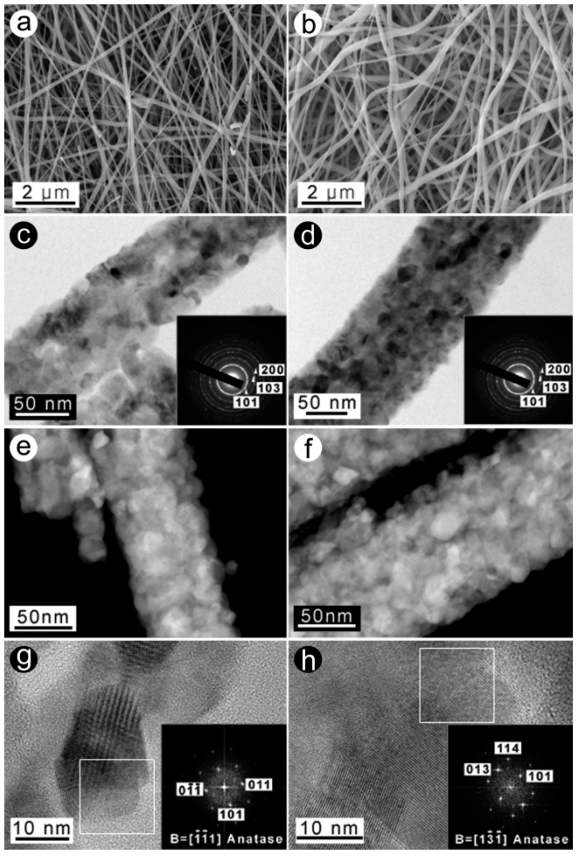

Figure 1. SEM images of (a) TiO_2 and (b) nitrogen-doped TiO_2 nanofibers after calcination. Bright-field TEM images of (c) TiO_2 and (d) nitrogen-doped TiO_2 nanofibers and their SAED patterns (inset), which correspond anatase phase. Annular dark-field STEM images of (e) TiO_2 and (f) nitrogen-doped TiO_2 nanofibers. HR-TEM images of (g) TiO_2 and (h) nitrogen-doped TiO_2 nanofibers and the corresponding FFT patterns.

of TiO_2 fibers mainly consisted of nanosized particles 10 nm in size. Moreover, the two types of fibers had typical mesoporous morphology, which is an ideal host for Li^+ intercalation, as shown by annular dark-field scanning TEM (STEM) images (Figure 1e, f). These fibers commonly also showed a random orientation and the lack of any impurity phases, as in the high-resolution TEM (HR-TEM) images g and h in Figure 1, and their fast Fourier transforms (FFT). It is worth noting that phases of bare and nitrogen-doped TiO_2 fibers also show no noticeable differences in X-ray diffraction (XRD) analysis (see Figure S3 in the Supporting Information). They both show only typical anatase phase without any impurity.

If nitrogen atoms are present in either interstitial or substitutional sites, a natural question is then where the nitrogen is. Very recently, TiO_2 hollow nanofibers were synthesized via the eletrospinning using a dual nozzle. These hollow nanofibers sheathed with TiO_xN_y and TiN layers on the surfaces were designed as a highly conducting layer for considering the dominant rate capability determining factors, i.e., lithium ion diffusivity, especially, solid-state diffusion of lithium ion, and electronic conductivity but nitrogen site was not still clarified.[31] To clarify the nitrogen site, we further investigated the surface of nitrogen-doped TiO_2 by energy-dispersive X-ray spectroscopy (EDS), Fourier transform infrared spectroscopy (FTIR), and X-ray photoelectron spectroscopy (XPS), as shown in Figure 2. First, we evaluated the presence of nitrogen doping by using EDS. According to the element mapping, we confirmed that the nitrogen was seen in nitrogen-doped TiO_2 nanofibers, as in Figure 2d. FTIR spectroscopy was then conducted. In the FTIR spectrum of nitrogen-doped TiO_2, there were three peaks at 470, 1630, and 3450 cm^{-1} (Figure 2e). These peaks are also observed in Degussa P25, which is composed of anatase and rutile crystallities, from earlier reports.[32] Interestingly enough, new peaks were found at 1460 and 2920 cm^{-1}, respectively (Figure 2e). The first peak (2920 cm^{-1}) can be related to the C−H vibration in remnant organic compounds in our TiO_2 nanofibers.[32] The small peak at 1460 cm^{-1}, which was produced by $-NO_x$ (−Ti−O−N−Ti−), indicated that nitrogen atoms in the nitrogen-doped TiO_2 sample existed in the form of $-NO_x$.[33] Even after EDS and FTIR, however, controversy still remains. In order to further clarify the nitrogen positions, XPS analysis was also undertaken. Based on literature surveys,[34−39] the broad peak at 398.2−400.7 eV can be interpreted as the result of nitrogen atoms occupying interstitial sites in the TiO_2 lattice (TiO_2N_x), whereas the peak at 396−397 eV could be derived from substitution of nitrogen on the oxygen site in TiO_2 ($TiO_{2-x}N_x$) or adsorbed NH_x species, i.e., molecular nitrogen on the surface.[35] In our study, N 1s was found to be around 400.0 eV, four peaks were also found from O 1s, as can be seen in Figure 2f, g. Two peaks of 532.0 and 533 eV were reported to be related to NO_x.[32] In addition, the peaks at 529.9 and 531.3 eV can be attributed to Ti−O bond and Ti−O−N bonds, respectively. Even if the spectra of O 1s observed at 531.8 eV was reported to be Ti oxynitride (TiO_xN_y),[40] neither TEM nor XRD (see Figure S3 in the Supporting Inforamtion) revealed any other evidence beyond anatase. The Ti oxynitride is well-known to be rock-salt crystal structure of osbornite. We thus consider either an interstitial or a substitution in anatase TiO_2.

To again confirm this issue, we carried out a series of first-principles calculations on the nitrogen-doped TiO_2 surface. Substitutional nitrogen doping was simulated by replacing one

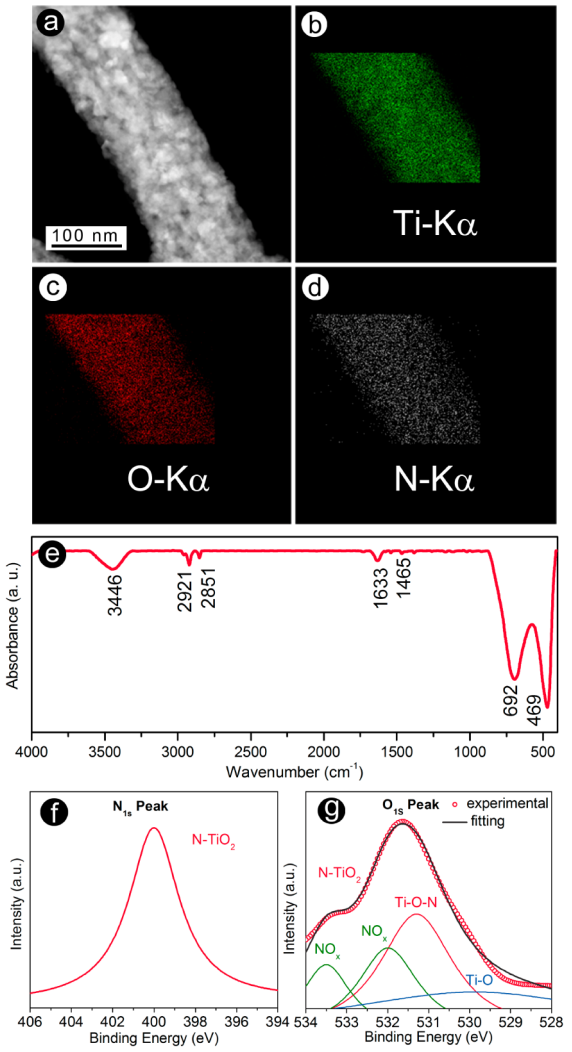

Figure 2. (a) TEM image of (a) nitrogen-doped TiO_2 nanofibers, (b) its titanium, (c) oxygen, and (d) nitogen mapping. FTIR spectrum of nitrogen-doped TiO_2 nanofibers (e). XPS spectra of nitrogen-doped TiO_2 nanofibers: (f) N_{1s} peak, (g) O_{1s} peak.

oxygen atom per supercell with a nitrogen atom, and interstitial nitrogen doping was simulated by adding one nitrogen atom to a neighboring site to an oxygen atom in the surface slab model: this corresponds to $TiO_{2-x}N_x$ (TiO_2N_x) with x = 0.021. Our main concern is to establish whether the nitrogen defect in the surface is favored with respect to that in a sublayer. To this end, various possible nonequivalent surface and subsurface substitutional nitrogen sites (Ns) and interstitial nitrogen sites (Ni) have been considered. For all Ns configurations, no significant structural variation is observed upon substitution: the Ti−N bonds are only slightly (less than 0.1 Å) elongated with respect to the corresponding Ti−O bonds. For the most stable interstitial doping, nitrogen atoms bond with three neighbors, one with surface oxygen (d_{N-O} = 1.27 Å) and the others with Ti atoms (d_{Ti-N} = 1.96 Å, 2.16 Å, respectively). The surface oxygen, when bonded with an N atom, was kicked out of the surface, ∼1 Å above the initial position. Figure 3a shows the relative defect energies (E_d) for various nitrogen atom positions. The defect energy of bulk TiO_2 in anatase phase and the height of the outermost oxygen atom in pristine (101) were set as the origin of the y-axis and abscissa, respectively.

dx.doi.org/10.1021/am302197y | ACS Appl. Mater. Interfaces 2013, 5, 691−696

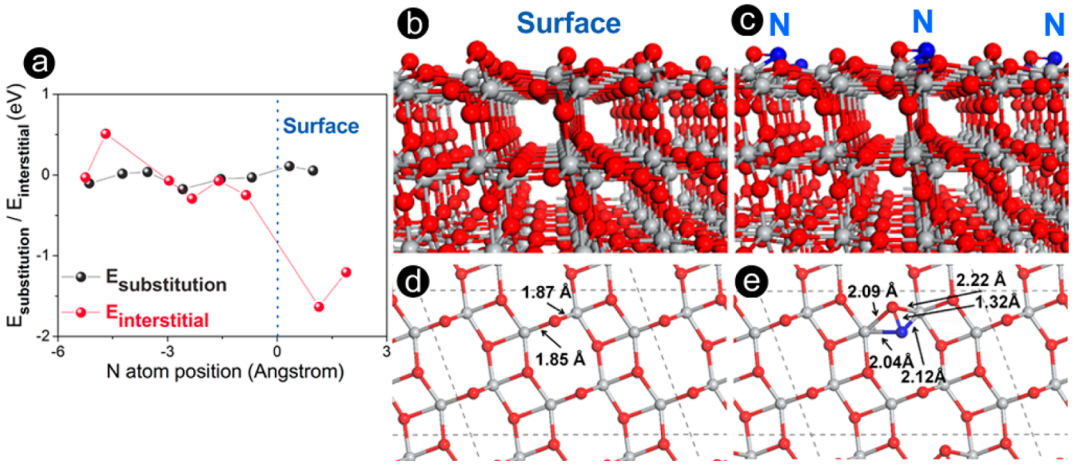

Figure 3. (a) Energetic graph of a nitrogen atom site, (b) geometry of the TiO_2 structure, and (c) interstitial sites on the surface of nitorgen-doped TiO_2 structure. (d, e) The atomic geometries are viewed in (001) direction for the corresponding samples. Herein dashed lines show the surface unit cell.

The nitrogen atom substitution occurs preferentially in the subsurface layer (−0.18 eV at 3.47 Å below the TiO_2 surface). On the other hand, the most stable interstitial nitrogen atom resides in a surface site (Figure 3c, e; −1.63 eV at 0.26 Å above the TiO_2 surface). That is, substitutional nitrogen would be spread widely in the bulk, while interstitial nitrogen atoms were mostly located near the surface.

We have also investigated the work function variation in each configuration (see Table SI in the Supporting Information). The work function is defined as the energy of the vacuum level (determined by applying a dipole correction to the super cell[41]) with respect to the Fermi energy, E_F, in each configuration. For the substitutional doping, the work function deviates a little (~0.3 eV) from that of the pristine surface (7.34 eV), although the work function of interstitial doping is much reduced (~1.3 eV) from that of the pristine surface. The high work function, i.e., the lower lying valence band maximum is the main obstacle to the use of TiO_2 as a photocatalyst or as an electrode of a photoelectrochemical (PEC) cell. Work function engineering by nitrogen interstitial doping may be valuable for various applications of TiO_2 material, such as in photocatalysis, PEC cells, and solar cells (see Figure S4 in the Supporting Information).

It is well-known that a small fraction of nitrogen doping as impurity in semiconductor material, especially TiO_2, can improve electrical conductivity. Here, we consider the internal conductivity as investigated by electrochemical impedance spectroscopy of TiO_2 nanoparticles, TiO_2 nanofibers and nitrogen-doped TiO_2 nanofibers, as shown in Figure 4. In the electrochemical impedance spectra (EIS) of TiO_2, the high frequency semicircle can be attributed to the contact resistance or the solid electrolyte interphase (SEI) film, the medium frequency semicircle indicates the charge transfer resistance at the interface between the electrolyte and the electrode material, and the inclined lines correspond to the Li^+ diffusion process inside the electrode material. When the experimental data was fitted using a typical equivalent circuit (shown in the inset of Figure 4), the different sizes of the semicircle among these materials were primarily associated not with contact resistance or SEI film, but with charge transfer resistance. So, the more restrained semicircle of bare TiO_2 nanofibers (1301 Ω) compared to that of TiO_2 nanoparticles (2370 Ω) clearly proves that the electrode materials with 1D structure feature

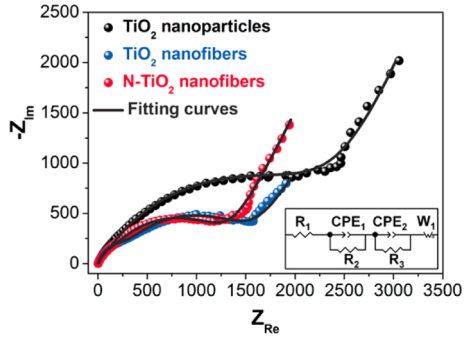

Figure 4. Nyquist plots of TiO_2 nanoparticles, TiO_2 nanofibers, and nitrogen-doped TiO_2 nanofibers. The inset figure corresponds to the equivalent circuit used to interpret the impedance spectra.

enhanced kinetic properties because of their innately conductive electronic structure.[42,43] Finally, the smallest resistance (1170 Ω) was observed in nitrogen-doped TiO_2 nanofibers confirms that the doped nitrogen results in enhancing electrical conductivity becaues of an electron acceptor.[36] Interestingly, the linear Warburg region (at low frequencies), which correspond to the Li^+ diffusion inside the electrode materials, for the nitrogen-doped TiO_2 nanofibers exhibit slightly steeper slope. That is to say, this result demonstrates that nitrogen doping plays an important role for fast charge transfer and Li^+ diffusion, which would affect electrochemical performance.

The electrochemical performance of the two different TiO_2 nanofibers for use as anode in the lithium rechargeable battery is shown in Figure 5. Anatase TiO_2 nanoparticles were also tested as a reference. More details on the sample preparation can be found in the Experimental Section. The galvanostatic profiles of the three TiO_2 configurations show a clear voltage plateau during Li^+ insertion/extraction, indicating that all TiO_2 samples have a typical anatase phase. The preferential use of anatase phase compared to rutile phase for the lithium rechargeable battery is due not only to the voltage plateau characteristics of anatase, but also to its better electrochemical performance, such as higher capacity and better cyclic retention. The nitrogen-doped TiO_2 nanofibers shown in Figure 5 have a specific charge (Li^+ insertion) capacity of around 224 mA h g^{-1}, and further cycling leads to around 185

dx.doi.org/10.1021/am302197y | ACS Appl. Mater. Interfaces 2013, 5, 691−696

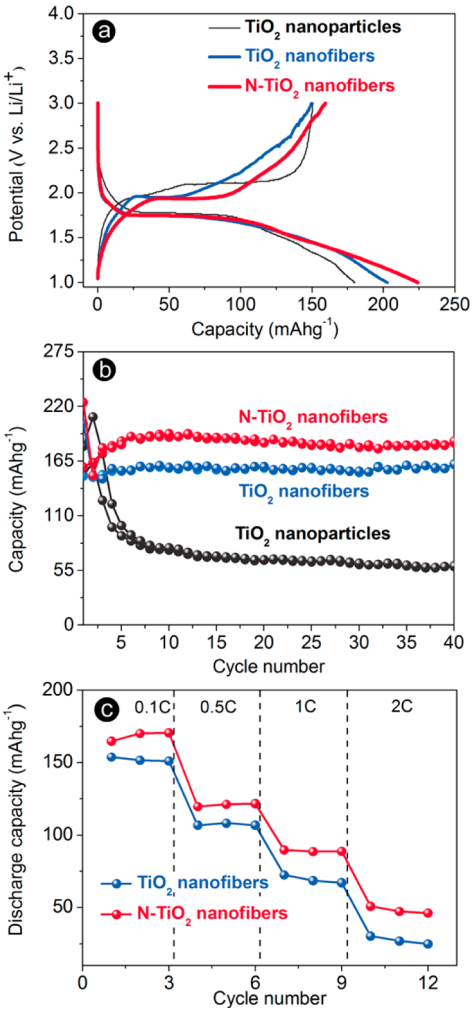

Figure 5. (a) Charge−discharge in the first cycle (0.1C) and (b) cyclic retention (0.1C) curves of TiO_2 nanoparticles, TiO_2 nanofibers, and nitrogen-doped TiO_2 nanofiber electrodes. (c) Rate performance of of TiO_2 nanofibers and nitrogen-doped TiO_2 nanofiber electrodes.

mA h g^{-1} retention after 40 cycles. This indicates that the superior cycling performance can be attributed to the morphological advantage for Li^+ storage as well as faster Li^+ diffusion. As pointed out by Park et al.[44] 1D nanostructures such as in urchin-like structures or nanorod structures on the surface of spherical particles can supply the most optimized environment for facilitating the charge/discharge process of Li^+ because of their dual merits, including a suitable surface area, excluding large irreversible capacity, and the high aspect ratio necessary for fast electron transport. After first cycle, the Coulombic efficiency of nitrogen-dpoed TiO_2 nanofiber and TiO_2 nanofiber is better compared to that of TiO_2 nanoparticle proving the enhanced reversibility associated with 1D structure (see Figure S5 in the Supporting Information). Furthermore, the comparison between nitrogen-doped TiO_2 nanofiber and bare TiO_2 nanofiber clearly proves the effect of nitrogen doping on the rate performance of TiO_2 in Figure 5c. The nitrogen-doped TiO_2 nanofibers show enhanced rate capability compared to bare TiO_2 nanofiber from 0.1 to 2C. This result indicates that nitrogen doping is contributed to fast Li^+ transfer and electron transfer with higher conductivity. Therefore, our mesoporous 1D structure results in higher specific surface area, strongly facilitating Li^+ diffusion, which produces enhanced cyclic retention.

CONCLUSIONS

We have undertaken 1D mesoporous TiO_2N_x and find that the microscopic and electronic origins for the enhancement of cyclic retention is due to higher conductivity and faster Li^+ diffusion, as confirmed by electrochemical impedance spectra and charge/discharge curve. The nitrogen interstitially located near surface in the form of TiO_2N_x, improving conductivity and changing work function, based on our first principles calculations. In addition, we answer the effect of nitrogen doping clearly: where does nitrogen, what is formed, and why electrochemical performance properties are improved? The nitrogen-doped TiO_2 nanofibers (185 mA h g^{-1}) show much higher cyclic retention than the nanopowders (60 mA h g^{-1}) after 40 cycles. It is proposed that rationalized nitrogen-doped 1D morphology facilitates the charge/discharge process of Li^+.

ASSOCIATED CONTENT

Supporting Information

Figures showing SEM images, XRD patterns, relative energies (eV) for Substitutional (Es) and Interstitial (Ei) Nitrogen in different positions of anatase TiO_2(001) surface slab model, the work function (eV) and N 1s core level shift (eV) and UV−vis spectra. This material is available free of charge via the Internet at http://pubs.acs.org.

AUTHOR INFORMATION

Corresponding Author

*E-mail: jhk@uow.edu.au (J.H.K.); dake1234@dongguk.edu (Y-.M.K.).

Author Contributions

†These authors contributed equally.

Notes

The authors declare no competing financial interest.

ACKNOWLEDGMENTS

This work is supported by an Australian Research Council Discovery Project (DP1096546). Y.-M.K. acknowledges the financial support by NRF-2010-C1AAA001-0029018 and the Basic Science Research Program (20090072972) through the National Research Foundation of Korea funded by the MEST. K.-J.K. acknowledges support through a grant from the R&D program for Energy Efficiency & Resources of the Korea Institute of Energy Technology Evaluation and Planning (KETEP) funded by the Ministry of Knowledge Economy, Republic of Korea. This paper was also studied with the support of the MEST (Ministry of Education Science and Technology) and KOFST (The Korean Federation of Science and Technology Societies).

REFERENCES

(1) Gratzel, M. *Nature* **2001**, *414*, 338−344.
(2) Bruce, P. G.; Scrosati, B.; Tarascon, J. M. *Angew. Chem., Int. Ed.* **2008**, *47*, 2930−2946.
(3) Hu, Y. S.; Kienle, L.; Guo, Y. G.; Maier, J. *Adv. Mater.* **2006**, *18*, 1421−1426.
(4) Ren, Y.; Liu, Z.; Pourpoint, F.; Armstrong, A. R.; Grey, C. P.; Bruce, P. G. *Angew. Chem., Int. Ed.* **2012**, *51*, 2164−2167.
(5) Armstrong, A. R.; Canales, J.; Garcia, R.; Bruce, P. G. *Adv. Mater.* **2005**, *17*, 862−865.

(6) Armstrong, G.; Armstrong, A. R.; Bruce, P. G.; Reale, P.; Scrosati, B. *Adv. Mater.* **2006**, *18*, 2597−2600.
(7) Kim, J.; Cho, J. *J. Electrochem. Soc.* **2007**, *154*, A542−546.
(8) Xu, J.; Jia, C.; Cao, B.; Zhang, W. F. *Electrochim. Acta* **2007**, *52*, 8044−8047.
(9) Bao, S.-J.; Bao, Q.-L.; Li, C.-M.; Dong, Z.-L. *Electrochem. Commun.* **2007**, *9*, 1233−1238.
(10) Reddy, M. A.; Pralong, V.; Varadaeaju, U. V.; Raveau, B. *Electrochem. Solid-State Lett.* **2008**, *8*, A132−A134.
(11) Noailles, L. D.; Johnson, C. S.; Vaughey, J. T.; Thackeray, M. M. *J. Power Sources* **1999**, *81*, 259−263.
(12) Kuhn, A.; Amandi, R.; Garcia-Alvarado, F. *J. Power Sources* **2001**, *92*, 221−227.
(13) Deng, D.; Kim, M. G.; Lee, J. Y.; Cho, J. *Energy Environ. Sci.* **2009**, *2*, 818−837.
(14) Brutti, S.; Gentili, V.; Menard, H.; Scrosati, B.; Bruce, P. G. *Adv. Energy Mater.* **2012**, *2*, 322−327.
(15) Jeong, G.; Kim, Y. U.; Kim, H.; Kim, Y. J.; Sohn, H. J. *Energy Environ. Sci.* **2011**, *4*, 1986−2002.
(16) Kim, J.; Cho, J. *Electrochem. Solid-State Lett.* **2007**, *10*, A81−A83.
(17) Prakash, A. S.; Manikandan, P.; Ramesha, K.; Sathiya, M.; Tarascon, J.-M.; Shukla, A. K. *Chem. Mater.* **2010**, *22*, 2857−2863.
(18) Laumann, A.; Boysen, H.; Bremholm, M.; Fehr, K. T.; Hoelzel, M.; Holzapfel, M. *Chem. Mater.* **2011**, *23*, 2753−2759.
(19) Xia, Y .; Yang, P.; Sun, Y.; Wu, Y.; Mayers, B.; Gates, B.; Yin, Y.; Kim, H.; Yan, H. *Adv. Master* **2003**, *15*, 353−389.
(20) Lu, X.; Wang, C.; Wei, Y. *Small* **2009**, *5*, 2349−2370.
(21) Shim, H. W.; Lee, D. K.; Cho, I. S.; Hong, K. S.; Kim, D. W. *Nanotechnology* **2010**, *21*, 255706−1−255706−9.
(22) Nam, S. H.; Shim, H. S.; Kim, Y. S.; Dar, M. A.; Kim, J. G.; Kim, W. B. *ACS Appl. Mater. Inter.* **2010**, *2*, 2046−2052.
(23) Li, D.; Xia, Y. *Adv. Master* **2004**, *16*, 1151−1170.
(24) Li, D.; Xia, Y. *Nano Lett.* **2004**, *4*, 933−938.
(25) Cojocaru, B.; Neatu, S.; Parvulescu, V. I.; Somoghi, V.; Petrea, N.; Epure, G.; Alvaro, M.; Garcia, H. *ChemSusChem* **2009**, *2*, 427−436.
(26) Kresse, G.; Furthmuller, J. *Phys. Rev. B* **1996**, *54*, 11169−11186.
(27) Kresse, G.; Furthmuller, J. *Comput. Mater. Sci.* **1996**, *6*, 15−50.
(28) Perdew, J. P.; Burke, K.; Ernzerhof, M. *Phys. Rev. Lett.* **1996**, *77*, 3865−3868.
(29) Blochl, P. E. *Phys. Rev. B* **1994**, *50*, 17953−17979.
(30) Kresse, G.; Joubert, D. *Phys. Rev B* **1999**, *59*, 1758−1775.
(31) Han, H.; Song, T.; Bae, J. Y.; Nazar, L. F.; Kim, H.; Paik, U. *Energy Environ. Sci.* **2011**, *4*, 4532−4536.
(32) Peng, F.; Cai, L.; Yu, H.; Wang, H.; Yang, J. *J. Solid State Chem.* **2008**, *181*, 130−136.
(33) Huang, D. G.; Liao, S. J.; Zhou, W. B.; Quan, S. Q.; Liu, L.; He, Z. J.; Wan, J. B. *J. Phys. Chem. Solids* **2009**, *70*, 853−859.
(34) Zhou, Z.; Huang, Y. *J. Phys.: Conf. Ser.* **2009**, *188*, 012033−012037.
(35) Asahi, R.; Morikawa, T.; Ohwaki, T.; Aoki, K.; Taga, Y. *Science* **2001**, *293*, 269−271.
(36) Batzill, M.; Morales, E. H.; Diebold, U. *Phys. Rev. Lett.* **2006**, *96*, 026103−1−026103−4.
(37) Han, K. S.; Lee, J. W.; Kang, Y. M.; Lee, J. Y.; Kang, J. K. *Small* **2008**, *4*, 1682−1686.
(38) Valentin, C. D.; Pacchioni, G.; Selloni, A.; Livraghi, S.; Giamello, E. *J. Phys. Chem. B* **2005**, *109*, 11414−11419.
(39) Lai, C.; Yuan, X. C.; X. Cao, L.; Qiao, Q. Q.; Wang, Y. L.; Yeb, S. H. *Electrochem. Solid-State Lett.* **2012**, *15*, A65−A67.
(40) Vitiello, R. P.; Macak, J. M.; Ghicov, A.; Tsuchiya, H.; Dick, L. F. P.; Schmuki, P. *Electrochem. Commun.* **2006**, *8*, 544−548.
(41) Neugebauer, J.; Scheffler, M. *Phys. Rev. B* **1992**, *46*, 16067−16080.
(42) Chan, C. K.; Peng, H.; Liu, G.; Mcilwrath, K.; Zhang, X. F.; Huggins, R. A.; Cui, Y. *Nat. Nanotechnol.* **2008**, *3*, 31−35.
(43) Mai, L.; Dong, Y.; Xu, L.; Han, C. *Nano Lett.* **2010**, *10*, 4273−4278.
(44) Park, J. C.; Kim, J.; Kwon, H.; Song, H. *Adv. Mater.* **2009**, *21*, 803−807.